Energy & Environmental Science

Cite this: *Energy Environ. Sci.*, 2012, **5**, 5370

www.rsc.org/ees

PAPER

Investigation of surface Sr segregation in model thin film solid oxide fuel cell perovskite electrodes

WooChul Jung†* and Harry L. Tuller

Received 27th September 2011, Accepted 25th October 2011
DOI: 10.1039/c1ee02762j

While SOFC perovskite oxide cathodes have been the subject of numerous studies, the critical factors governing their kinetic behavior have remained poorly understood. This has been due to a number of factors including the morphological complexity of the electrode and the electrode- electrolyte interface as well as the evolution of the surface chemistry with varying operating conditions. In this work, the surface chemical composition of dense thin film $SrTi_{1-x}Fe_xO_{3-\delta}$ electrodes, with considerably simplified and well-defined electrode geometry, was investigated by means of XPS, focusing on surface cation segregation. An appreciable degree of Sr-excess was found at the surface of STF specimens over the wide composition range studied. The detailed nature of the Sr-excess is discussed by means of depth and take-off angle dependent XPS spectra, in combination with chemical and thermal treatments. Furthermore, the degree of surface segregation was successfully controlled by etching the films, and/or preparing intentionally Sr deficient films. Electrochemical Impedance Spectroscopy studies, under circumstances where surface chemistry was controlled, were used to examine and characterize the blocking effect of Sr segregation on the surface oxygen exchange rate.

1. Introduction

Concerns about the environmental consequences of fossil fuel combustion have stimulated interest in developing alternative environment-friendly energy sources. Amongst the various means for achieving improved energy conversion efficiency, the solid oxide fuel cell (SOFC) has received much attention given its high potential conversion efficiency, the flexibility that it offers with respect to fuel choices (hydrocarbons as well as hydrogen) and the reduced emissions associated with electrochemical energy conversion devices.[1]

While SOFC metal oxide cathodes have been the subject of numerous studies, the mechanisms controlling their behavior have remained poorly understood.[2–7] This has been due to a number of factors, including the morphological complexity of the electrode and the electrode- electrolyte interface,[8] the evolution of the surface chemistry with varying operating conditions,[9,10] and the difficulty in interpreting electrochemical properties with multiple processes involved.[11] In this work, dense thin film $SrTi_{1-x}F_xO_{3-\delta}$ (STF) electrodes, with considerably simplified and well-defined electrode geometry and electrode-electrolyte interface, were chosen as a model, representing mixed ionic electronic conducting (MIEC) perovskite oxide cathodes. The surface chemical composition of the STF thin films is investigated by means of X-ray photoelectron spectroscopy (XPS), focusing on surface cation segregation. The detailed nature of the surface segregation is discussed in terms of layer formation, structure, and possible driving forces. In addition to XPS, morphological and electrochemical properties are examined by Atomic Force Microscopy (AFM) and Electrochemical Impedance Spectroscoty (EIS), respectively, providing improved insight into the role of surface cation segregation on the SOFC cathode reaction rate.

Department of Materials Science and Engineering, Massachusetts Institute of Technology, Cambridge, MA 02139, USA. E-mail: wcjung@mit.edu; Fax: +1-617-258-5749; Tel: +1-617-253-2364
† Current address: Applied Physics and Materials Sciences, California Institute of Technology, Pasadena, CA 91125, USA.

Boarder context

Solid oxide fuel cells (SOFCs) are expected to play a major role in a sustainable energy future given their high potential conversion efficiency. A key challenge hindering SOFC development is the limited degree of understanding regarding the kinetics of the cathode processes and the resultant efficiency loss. Here, concurrent studies of chemical, morphological and electrochemical properties of a model cathode system, with well-defined thin film geometry, revealed the detailed nature of surface chemical segregation and its influence on cathode kinetics, providing guidance for high performance SOFC cathodes.

2. Experimental

2.1. Sample preparation

STF thin films were prepared by means of pulsed laser deposition (PLD) from oxide targets of the respective materials and deposited onto (100) oriented single crystal yttria doped zirconia (YSZ) substrates for EIS measurement. One inch diameter oxide targets were prepared by the conventional mixed-oxide technique starting from iron(III) oxide (Alfa Aesar, 99.945%), strontium carbonate (Alfa Aesar, 99.99%), and titanium(IV) oxide (Alfa Aesar, 99.9%) powders. A Coherent (Santa Clara, CA) COMPex Pro 205 KrF eximer laser, emitting at a wavelength of 248 nm, was used for ablation. The deposition parameter configuration was 400 mJ/pulse laser energy, 8 Hz laser repetition rate, and an O_2 working pressure of 10 mTorr. Film thicknesses ranging between 100 and 500 nm were determined by surface profilometry (Tencor P-10). Detailed information regarding oxide target preparation and PLD deposition conditions can be found in previous studies.[12,13]

2.2. Physical and chemical characterization

X-ray diffraction (XRD) measurements were performed on synthesized powders and deposited films using a Bragg-Brentano diffractometer (Rigaku RU300, Tokyo, Japan, Cu-Kα wavelength ($\lambda = 1.541$ Å)), indicating the films to be polycrystalline perovskite phase with highly (110) oriented texture over the whole range of Fe fraction. Limited reflections from (100) or (111) are sometimes observed above background noise level. There is no evidence of amorphous films, or diffraction peaks other than the ones in the cubic perovskite phase.[14] The grain size, morphology, and surface roughness of the STF thin films were characterized by a Vecco Metrology (Santa Barbara, CA) D3000 atomic force microscope (AFM) with a Nanoscope IIIa controller. Micrographs were analyzed to determine the root mean square (RMS) surface roughness and grain size using Vecco's Nanoscope software (version 5.12r3). The chemical composition of the sample surfaces were measured in a Kratos Analytical (Manchester, UK) model Axis Ultra X-ray photoelectron spectrometer. A monochromated aluminum X-ray source of 1486.6 eV was used at a power of 150 W. Pass energy of 160 eV and 20 eV were used for survey and high resolution scans, respectively. Binding energy values were calibrated by setting the peak energy of the 1s electron in carbon, found as a surface contaminant in open air, to 285.0 eV. For depth-dependent composition determination, an Ar ion beam of 4 kV was used with 2×2 mm^2 rastering area.

2.3. Electrochemical measurements

A symmetrical structure, with identically sized STF electrodes on both sides of the YSZ electrolyte, was used for EIS measurements. Au mesh and Au paste were placed on each STF electrode surface, serving as current collectors. In order to confirm that any possible interactions between the Au and the oxygen did not influence the impedance spectra, photo-lithographically defined platinum patterns were sometimes fabricated between the YSZ substrate and the STF film, serving as a buried current collector. Both a custom-designed enclosed probe station, manufactured by McAllister Technical Services (Coeur d'Alene, ID) and a tube furnace were used for the EIS measurements at temperatures between 485 °C and 560 °C in air. EIS measurements, covering the frequency range from 7 mHz to 1 MHz, with amplitude of 20 mV, were performed with a Solarton 1260 or 1250 impedance analyzer operated in combination with a Solartron 1286 potentiostat/galvanostat.

3. Results

3.1. Surface morphologies of STF thin films

An AFM image of the surface of an as-deposited $SrTi_{0.5}Fe_{0.5}O_{3-\delta}$ film, designated as STF50, is shown in Fig. 1a. The lateral dimensions all span 1μm. The vertical dimension for the image is indicated on the z-axis scale as ~10 nm. The STF film deposited at 700 °C onto a YSZ single crystal substrate (100, MTI Corporation) exhibited grain sizes in the range of 100–200 nm and an RMS surface roughness of less than 1 nm (*e.g.*, 0.75 ± 0.12 nm) for a 500 nm thick layer, indicative of a highly smooth surface.

Surface morphological changes, induced by chemical and thermal treatments, in the films were also investigated. In this case, the STF film was etched by a 10% diluted buffered HF (NH_4F : HF = 7 : 1) solution for 20 s. Etch concentration and time for the etching process were chosen to remove a surface layer thickness between 5 and 10 nm, based on an average etch rate of ~0.4 nm s^{-1}. Fig. 1a-b provides AFM images of the STF50 film before and after chemical etching with the etching procedure increasing the roughness as illustrated. However, the change in the total surface area is estimated to change by only a few percent (see Table 1).

After etching, the sample was then subsequently annealed during the impedance measurements between 485 and 560 °C in air. Lastly the sample was annealed at high temperature for longer period of time (650 °C for 5 h). The corresponding AFM images are shown in Fig. 1c-d. Following heat-treatment, the surface morphology becomes more rounded with some abnormally large grains developing. In general, surface roughness increases following chemical etching and heat-treatment. The RMS roughness of the film following etching and heat-treatment is calculated to be four times higher than that of the as-deposited film, while the change in the total surface area still falls within only a few percent of the initial value (see Table 1).

3.2. Surface chemical compositions of STF thin films

3.2.1. Surface Sr-Excess. An appreciable degree of Sr-excess, near the surface, was found by means of XPS, known to be extremely sensitive to the near-surface region, over the whole composition range studied. Fig. 2a shows the ratio between Sr and the other cations (A-site to B-site cation ratio). This ratio is unity in an ideal stoichiometric perovskite structure. However, it was generally found to be greater than one, with values reaching approximately three at large Fe fractions on the B-site, indicating Sr-excess near the surface. On the other hand, the B-site cations largely maintain their designated ratio (Ti/Fe) as in the bulk (see Fig. 2a (insert)).

Angle resolved measurements were also performed to obtain depth dependent information (see Fig. 2b). These spectra were

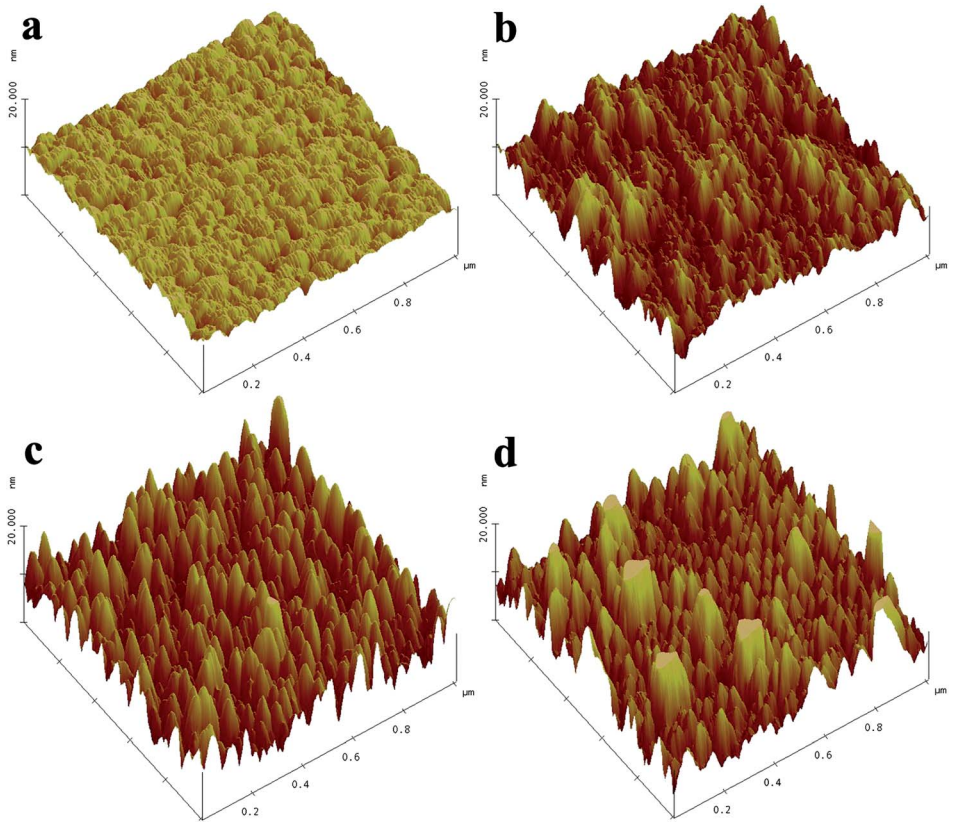

Fig. 1 AFM micrograph of STF50 surfaces before (a) and after (b) acid etching, and subsequent annealing at (c) ~550 °C and (d) 650 °C for 5 h.

Table 1 Calculated RMS surface roughness and actual surface area in 1 mm × 1 mm, determined by AFM data analysis

	Surf. roughness (nm)	Surf. area in 1 mm × 1 mm (mm^2)
As-deposited	0.78 ± 0.08	1.0032
After etching	2.00 ± 0.32	1.0173
Thermal cycles	2.95 ± 0.34	1.0344
Post-annealing	3.28 ± 0.35	1.0287

measured at the two different take-off angles of 0 and 70°. The measured level of Sr-excess increases as the take-off angle is increased from 0 to 70 °C. Since higher take-off angle leads to shallower detecting depth, this result is consistent with Sr-excess existing largely very close to the surface.

Fig. 3 shows O1s XPS peaks with an energy range between 536 and 526 eV. There are three different oxygen peaks (oxygen chemistry) observed in Fig. 3a. The main O 1s peak, at a binding energy of 529 eV, is ascribed to the strontium titanate oxygen ($SrTiO_3$), while the other peaks at binding energies of 531.8 and 534 eV correspond to hydroxyl and carbonate species, respectively.[15] There was no evidence of metallic Sr at the surface. Following Ar-ion milling of 20 s, corresponding to a removal of a 0.6 nm thick STF layer, both oxygen peaks related to $Sr(OH)_2$ and $SrCO_3$ largely disappear as evident in Fig. 3b.

XPS results as a function of a depth through the STF50 film by Ar-ion milling are shown in Fig. 4. The Sr content with respect to the other cations decreases as a function of depth and reaches nearly the stoichiometric composition, *i.e.*, Sr/(Ti + Fe) = 1, deep within the film. The depth of the heavily Sr enriched region extends to about 10 nm from the surface.

3.2.2. Modifications of surface Sr-Excess levels. To examine the role of surface segregation on the SOFC cathode reaction rate, the degree of segregation was carefully controlled, by etching the STF thin films, and/or preparing intentionally Sr deficient films by means of PLD. Since Sr segregation takes place only adjacent to the film surface, while the cation stoichiometry maintains deeper inside the film, nearly every etchant used in this study reduced the surface Sr excess, except for high concentration HF solutions (see Fig. 5a). Reactive ion etching (RIE) with Cl_2 gas also reduced the degree of Sr excess. 3% Sr-deficient STF ($Sr_{0.97}Ti_{0.5}Fe_{0.5}O_{3-\delta}$), selected because it is the maximum Sr deficiency compatible with the cubic perovskite structure, also exhibited a much reduced degree of Sr segregation. Fig. 5b shows the effect of chemical etching on the two extremes of Fe percent substituted for Ti in these studies. While a small decrease in Sr is observed for STF5, it is much more evident for STF100, where the Sr segregation is much stronger.

Re-segregation, induced by post-annealing etched specimens, was also observed. After being etched in diluted HF solution for 20 s, each STF50 sample was rapidly heated to 400 °C, 500 °C, and 650 °C, respectively, and quenched after annealing for two hours at the respective temperature. As shown in Fig. 6, the Sr-to-(Ti + Fe) ratio for the etched specimen maintains nearly the same value up to 500 °C, while it increases again after annealing at 650 °C, indicating that the Sr re-distribution is kinetically

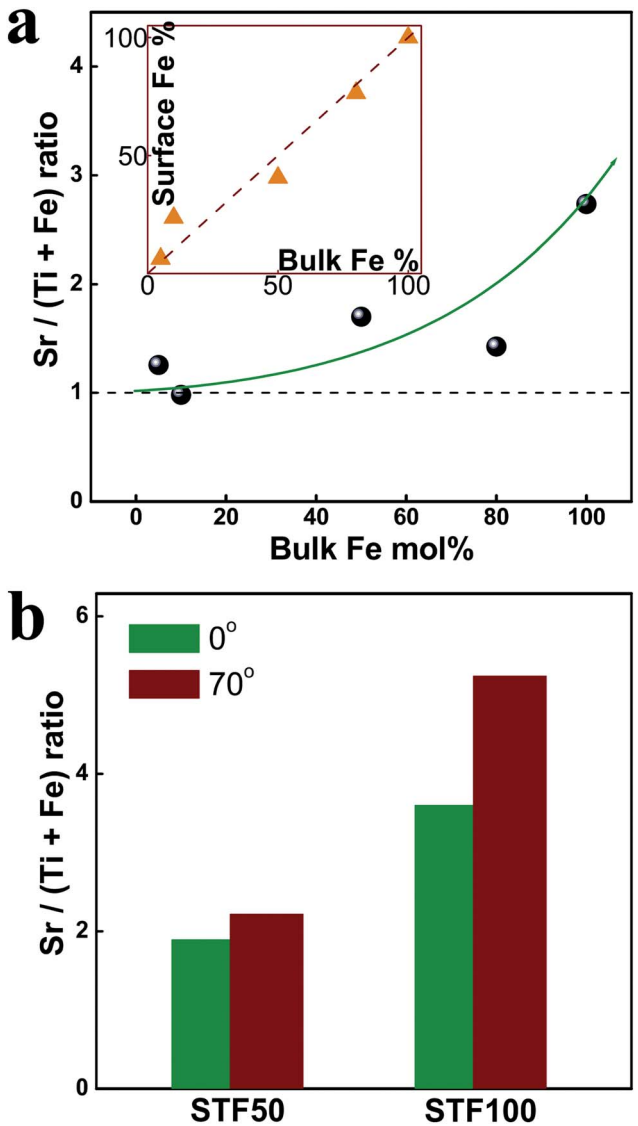

Fig. 2 (a) Ratio between A- and B-site cations as a function of Fe fraction, measured by XPS. (Insert) Surface *vs.* bulk Fe mol fraction with respect to the total B-site cations. (b) Ratio between A- and B-site cations measured at two different take-off angles of 0 and 70° for 50 and 100 mol% Fe.

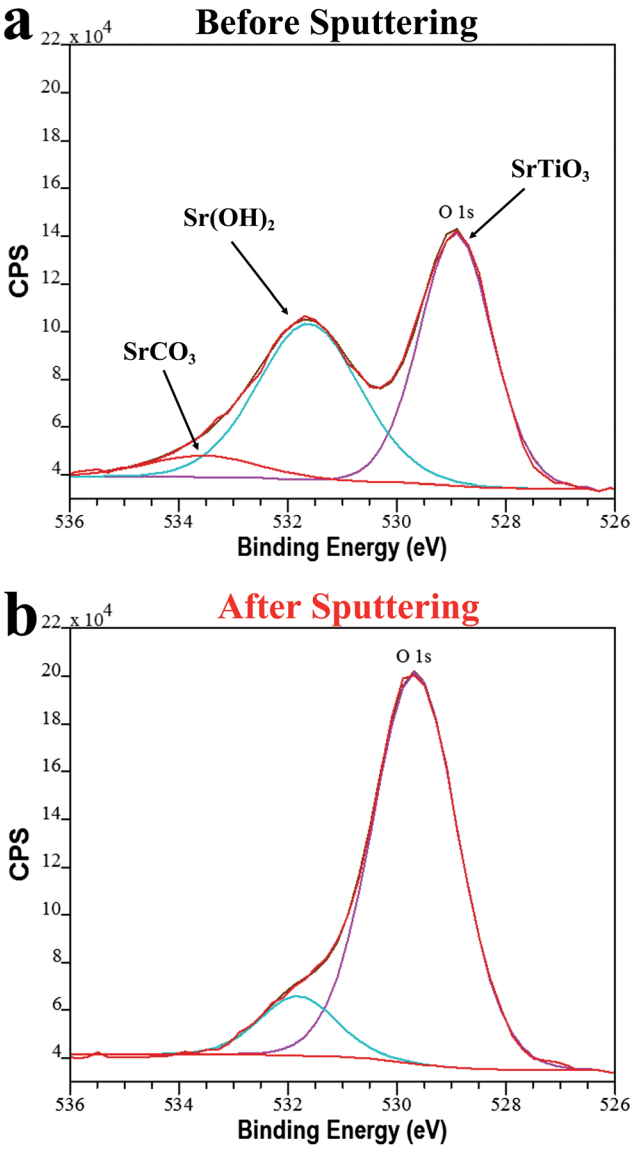

Fig. 3 Oxygen 1s spectra for as-deposited STF50 film before (a) and after (b) Ar-ion milling of 20 s.

hindered at temperatures of less than 500 °C. However, the Sr-to-(Ti +Fe) ratio remains the same even at 650 °C in case of the Sr deficient film, suggesting that the reduced Sr segregation for this material may be thermodynamically stable over the tested temperature range.

3.3. Electrochemical properties of STF thin film electrodes

3.3.1. Analysis of electrochemical impedance spectroscopy. In this work, a symmetrical structure with identically sized (9 mm × 9 mm) STF thin film electrodes on both sides of the YSZ electrolyte was prepared for EIS measurements. Previously, the resistance values derived from the STF electrode impedance were examined by their geometrical dependence on film thickness, electrode radius and the insertion of a CGO interlayer. Based on these measurements, it was conclusively concluded that the impedance governing process must be attributed to the oxygen exchange reaction occurring at the surface of the STF electrodes. For a detailed discussion of how the impedance spectra of these thin film structures were analyzed, the reader is referred to previous publications by the authors.[12–14]

The area specific electrode resistance R_{STF}, obtained by EIS measurements in air, was measured before and after etching and is plotted as a function of reciprocal temperature in Fig. 7. Since the STF electrode resistance is governed by the surface oxygen exchange reaction, R_{STF} is an indicator of how slow or fast oxygen surface exchange takes place on the STF electrode. It turns out that etching reduces the magnitude of R_{STF} over all Fe compositions studied in this work. In case of $SrFeO_{3-\delta}$, designated as STF100, nearly an order of magnitude decrease in R_{STF} was obtained (Fig. 7b). To examine the thermal stability of the etched film, the impedance was repeatedly measured over six

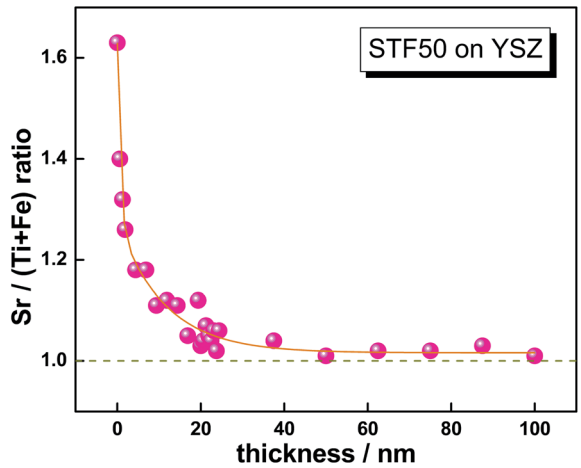

Fig. 4 Depth dependent chemical composition obtained for STF50. Ratio between Sr and (Ti + Fe) *vs.* depth from surface.

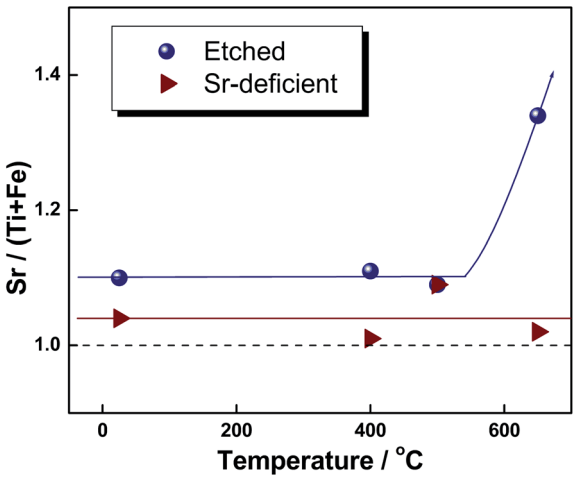

Fig. 6 Effect of post-annealing on the chemically etched STF film (circles) and the Sr deficient film (triangles).

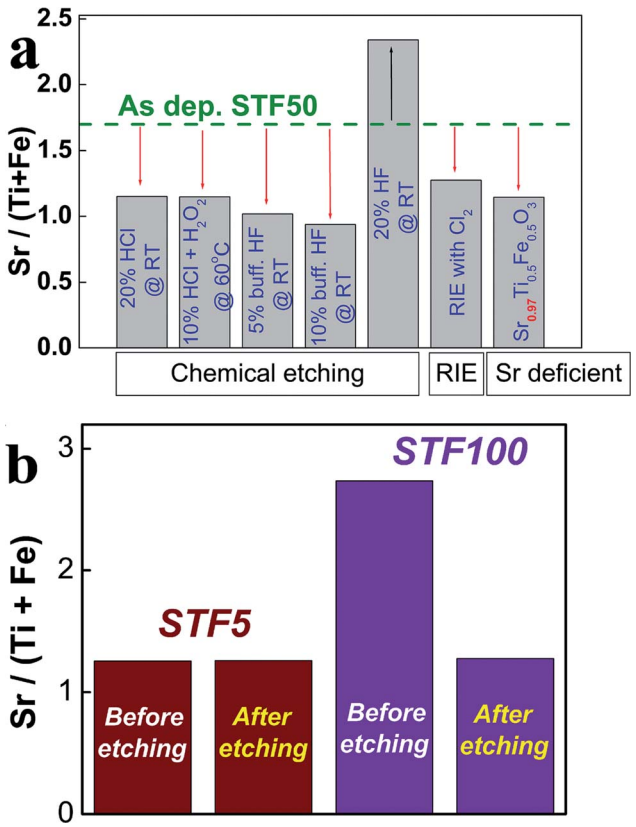

Fig. 5 (a) Changes in the ratio between A- and B-site cations for STF50 after etching the surface of the films or by preparation of Sr deficient film. (b) Changes in the ratio between A- and B-site cations for STF5 and 100 after etching the surface of the films by a 10% diluted buffered HF (NH_4F:HF = 7 : 1) solution for 20 s.

thermal cycle periods, *i.e.* one cycle includes heating-up and cooling-down between 485 and 560 °C. No significant differences in the impedance results were observed. However, after subsequent annealing at 650 °C for five hours, the resultant impedance increases, approaching the original un-etched values.

4. Discussion

4.1. Surface Sr segregation

4.1.1. Formation and structure of the segregated Sr layer. In order to understand the nature of the Sr excess at the surface, its formation is considered first. In principle, Sr can segregate as the oxide (SrO), as a reconstructed Sr excess phase ($SrO \cdot n(SrTiO_3)$), and/or as reaction products formed with chemi-adsorbed gases ($SrCO_3$ or $Sr(OH)_2 \cdot \times H_2O$). XPS revealed oxygen and strontium peaks corresponding to SrO (or $SrTiO_3$), hydroxyl species ($Sr(OH)_2$) and carbonate species ($SrCO_3$), respectively (see Fig. 3).[15–17] Given the similar structural nature and relatively large deviations between reported data for SrO and $SrTiO_3$ binding energies, it was not possible, on this basis, to distinguish between Sr as part of SrO *versus* $SrO \cdot n(SrTiO_3)$ or $SrTiO_3$ species. Fig. 3b demonstrates that the XPS peaks corresponding to the reaction compounds largely disappear following removal of approximately two atomic layers of the STF surface, while the respective oxide peaks remain. This is a clear indication that these reaction products ($(Sr(OH)_2)$ and $(SrCO_3)$), remain limited to the outermost STF layer and that most of the Sr segregation represents the formation of SrO, noting that Sr excess exists for more than ~10 nm in depth (see Fig. 4). It is reasonable to exclude a role for the reaction products on the impedance studies given that these speices are known to be removed from the $SrTiO_3$ surface upon heat-treatment,[18–20] under conditions comparable to those found under SOFC operation. One can also exclude the possibility of finding metallic Sr at the surface of the STF films, consistent with recent theoretical calculations reporting that pure Sr is highly unlikely on $SrTiO_3$ surfaces.[21] Therefore, it can be concluded that the surface Sr excess is largely a result of Sr segregation in the form of SrO or $SrO \cdot n(SrTiO_3)$.

Sr excess on $SrTiO_3$ has been extensively studied with three different species reported: SrO island precipitation,[21–23] SrO excess in a cubic perovskite phase ($SrTiO_3$),[24–27] and a reconstructed Sr excess phase ($SrO \cdot n(SrTiO_3)$).[25–29] Except for island formation, the other structures require a certain solubility of SrO in $SrTiO_3$. Both experimental observations and numerical calculations demonstrate that the cubic perovskite structure can

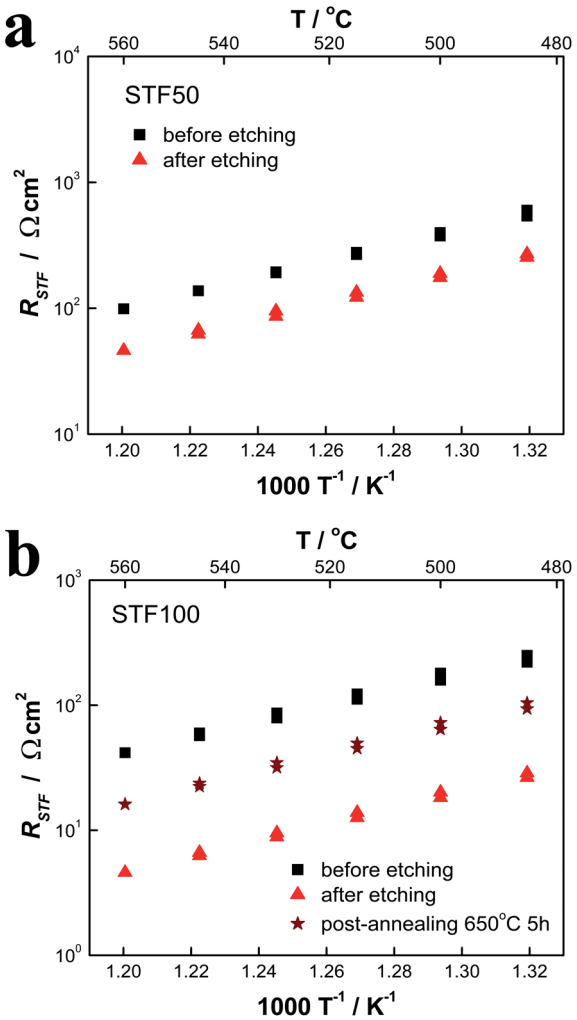

Fig. 7 Change in R_{STF} upon chemical etching. (a) Temperature dependence of R_{STF} for STF50 before (black square) and after (red triangle) etching with corresponding activation energies of 1.26 ± 0.02 eV and 1.26 ± 0.03 eV, respectively. (b) Temperature dependence of R_{STF} for STF100 before (black square), after (red triangle) etching, and after subsequent annealing at 650 °C 5h (brown star) with corresponding activation energies of 1.27 ± 0.04 eV, 1.30 ± 0.03 eV, and 1.31 ± 0.04 eV, respectively.

accommodate only limited amounts of excess SrO in the form of a solid solution,[24–27,30] *i.e.*, less than 0.2 mol% SrO in reference.[30] Likewise, the majority of literature suggests that the incorporation of planar defects in the form of rock salt structured layers is the likely mechanism for accommodating SrO excess. These planar defects, reflecting the additional SrO interlayers, lead to the formation of a structurally reconstructed Sr excess phase ($SrO \cdot n(SrTiO_3)$), often referred to as "Ruddlesden-Popper (RP) phases." Indeed, RP phases have been found, not only in SrO excess $SrTiO_3$ systems, but also in pure $SrTiO_3$ systems including single crystal $SrTiO_3$. Surface RP phases in $SrTiO_3$, or related doped systems, were observed by several surface characterization techniques including XPS,[31] STM,[32] neutron diffraction, TEM,[33] AFM,[28] and combined XRD & SIMS,[29] Therefore, given the large Sr excess found in this study, one can assume that the Sr excess is largely accommodated by the formation of RP phases or SrO island precipitates together with some amount of the RP phases.

4.1.2. Driving force for Sr segregation. Even though segregation of Sr in Sr rich perovskites is well known in the literature, the driving force for segregation remains unclear. Among several suggested models,[28,34,35] Szot reported that only kinetic demixing can account for such changes on a macroscopic scale in ternary oxides, *i.e.*, for distance greater than 10 nm.[28] This is based on the differences in mobility of the involved cations under an applied gradient; either thermal, electrical, mechanical, or chemical in nature.[36,37] For $SrTiO_3$, Wang and coworker have shown that the density of dislocations is unusually high in the 'skin' region of cut and unannealed single crystals.[38] They suggested that these extended defects not only act as fast diffusion paths for a redistribution of cations, predominantly Sr, within the near-surface region, but are accompanied by a strained region. This may be sufficient for the local mechanical stress gradients to act as driving force for the segregation of cations. Szot and coworkers reported rather direct evidence for this by AFM and EDX measurements on mechanically deformed single crystal $SrTiO_3$ surfaces at elevated temperature.[28] They concluded that mechanical stress leads to a massive segregation of Sr and subsequent recrystallization at the surface. Indeed, elasticity-induced solute redistribution around dislocations have been discussed in the literature (see[39] and references therein).

Furthermore, Sr, large in diameter, is normally surrounded by twelve oxygen atoms in the cubic perovskite lattice, *i.e.*, radius of 0.144 nm (Sr^{2+} for coordination number of 12) and 0.140 nm (O^{2-} for coordination number of 6),[40] and is therefore under high compressive stress. This lattice strain was thought to be the main source for chemical instability of the Sr containing perovskites. For example, the chemical compatibility of these perovskite oxides with YSZ could be significantly enhanced by adding a smaller size A-site cation such as La, or intentionally preparing the oxide with Sr deficiency.[41] Similar observation regarding the enhanced chemical compatibility with YSZ has also been reported even in the STF system with $Sr_{0.9}Ti_{0.6}Fe_{0.4}O_{3-\delta}$, $Sr_{0.97}Ti_{0.6}Fe_{0.4}O_{3-\delta}$, and $La_{0.4}Sr_{0.5}Ti_{0.6}Fe_{0.4}O_{3-\delta}$.[42]

Therefore, kinetic demixing, driven by mechanical strain gradients, may be considered as a relevant driving force for surface SrO segregation. In fact, since the lattice constant of STF decreases with increasing Fe,[43] more Fe is expected to create a higher degree of compressive strain on Sr atoms. Therefore, it may explain why higher Fe content in STF results in more Sr segregation. This concept is also supported by the fact that the 3% Sr deficient STF sample demonstrated a significantly reduced degree of Sr segregation in this work (see Fig. 5). Upon post annealing, no additional segregation was found on the Sr deficient STF film, indicating that the strain effect might be a thermodynamic driving force. However, with the limited number of experimental results obtained in this study, it is not possible to make a firm conclusion about the very nature of the Sr excess at the surface of the STF film, and further investigation will be required.

4.2. Role of Sr segregation on the rate of surface oxygen exchange

Surface segregation by A-site cations in perovskite materials has been frequently reported. This has included the SOFC cathode

materials such as (La,Sr)MnO_3 (LSM),[10,31,44,45] although the exact role of surface segregation on cathodic performance has not been fully understood. Surface exchange kinetics of LSM films have been reported to be depressed by Sr segregation due to the insulating nature of the SrO species.[44] On the other hand, the addition of SrO to the surface of undoped and lightly-Fe-doped $SrTiO_3$ have been reported to enhance the surface exchange reaction.[46] Recently, a small amount of secondary phase on $La_{0.8}Sr_{0.2}CoO_3$ (LSC) surface has been reported to either significantly activate or passivate the exchange rate.[47] In this study, the EIS data, under circumstances where a few top atomic layers were removed by chemical etching with dilute HF solution, reveal that the SrO segregated layer has a negative impact on the oxygen exchange rate. Nearly an order of magnitude decrease in R_{STF} was obtained by etching the surface of STF100, indicating that SrO excess acts as a passivation barrier for the surface oxygen exchange reaction. These findings would be consistent with the poor conducting properties of SrO, a wide bandgap insulator with E_g of $\sim$ 6 eV. The RP phases (SrO rich), on the other hand are generally not highly insulating.[48–50] For example, σ_{el} of 9.1 S cm^{-1} and σ_{ion} of 5.8 $\times$ 10^{-3} S cm^{-1} are reported for $Sr_3Fe_2O_{6+\delta}$, compared to 56.5 S cm^{-1} and 0.5 S cm^{-1}, respectively for its counterpart $SrFeO_{3-\delta}$ at 800 °C in air.[50] This does not, however, take into account potential barriers which may result from space charge fields generated between the perovskite STF and the additional surface RP phase layers.

Since chemical etching also induces changes in the surface morphology of the STF films, *i.e.* active surface area (see Fig. 1), one should also consider the potential impact of this on the impedance measurements, in addition to the removal of the SrO-rich phase. Based on an AFM analysis, the change in total surface area by etching and post-annealing was found to be only $\sim$3% (see Table 1). Furthermore, R_{STF} remained nearly constant upon repeated etching, as well as multiple heating and cooling cycles as long as the maximum temperature was maintained at < 560 °C, suggesting as well, that negligible re-segregation occurred during these subsequent thermal cycles. However, R_{STF} did increase, following post-annealing at higher temperature (650 °C) for five hours, approaching the original non-etched value (see Fig. 7b). Therefore, one can conclude that R_{STF} change can be largely attributed to surface segregation with the "SrO" excess layer serving as a barrier for oxygen exchange.

Previously, these authors revealed a strong correlation between the position of the Fermi energy relative to the conduction band edge and the activation energy exhibited by the surface oxygen exchange rate constant in STF thin film electrodes, confirming experimentally, *for the first time*, the key role that the minority electronic species play in determining the overall reaction kinetics.[14] Accordingly, the change in R_{STF} should be understood in the context of the electron charge transfer efficency from the STF oxide to the adsorbed oxygen species at the surface. Noting further that the activation energy for R_{STF} remains nearly unchanged, within $\pm$ 0.3 eV, upon chemical etching, one can assume two possible situations regarding the role of Sr excess at the surface, as shown in Fig. 8. (1) The "SrO" layer covers nearly the entire STF cathode surface uniformly, leaving only microscopic or nanoscopic porosity enabling oxygen to exchange between the gas phase and the STF electrode, albeit at a markedly decreased effective surface area.

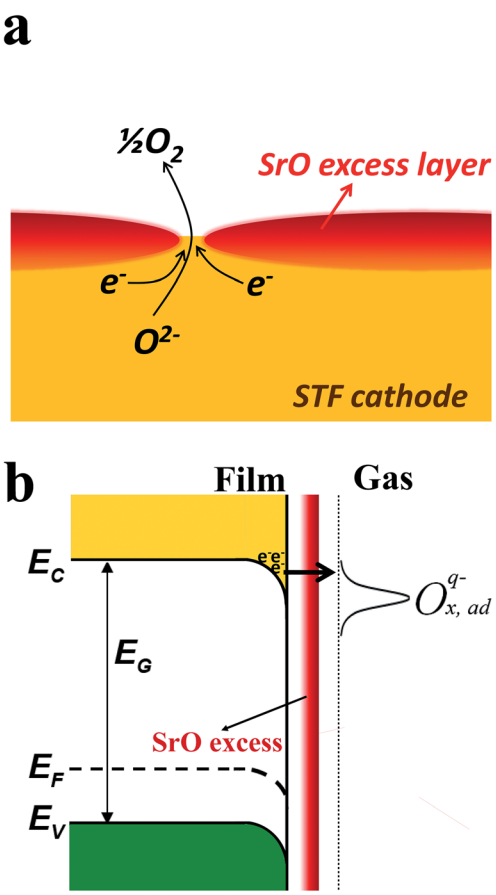

Fig. 8 Possible "SrO" passivation mechanisms. (a) "SrO" rich layer acting as blocking barrier to oxygen molecules accessing the active STF surface except *via* pinholes in the SrO layer. (b) Thin, dense "SrO" rich layer limiting electron transfer to "tunneling" from active STF surface to adsorbed oxygen.

Inhomogeneous coverage could result from differences in segregation at grains with differing crystallographic orientation or preferential segregation at grain boundaries. (2) Electron charge transfer takes place through a pin-hole free "SrO" layer by a predominantly non thermally activated tunneling process.

The surface exchange rate was found to be only weakly dependent on Fe fraction in STF, *e.g.* within a factor of 2, in going from STF35 and STF100.[14] This is the case in spite of the fact that STF100 has 100, 20, and 200 times higher σ_{el}, σ_{ion}, minority carrier density (n), respectively, compared with STF35. This relative insensitivity of the surface exchange rate to the Fe fraction may be attributed to the passivation effect of the "SrO" layer. As demonstrated above, the degree of Sr segregation increases with increasing Fe fraction (see Fig. 2a) which would be consistent with either of the two models suggested above for contributing to the reduction in oxygen exchange rate relative to what one could expect, *i.e.* reduction in porosity or increase in layer thickness. As noted above, both models are consistent with the observation that the "SrO" excess layer has little influence on the activation energy of the surface exchange reaction.

The fact that the segregated "SrO" layer depresses the oxygen exchange rate, suggests that SOFC performance could be improved by removing surface passivation layers or selecting

electrode compositions not susceptible to Sr segregation. Controlling the surface chemistry may not be easy, considering the high operating temperatures of conventional SOFC systems and the resultant potential for thermal re-segregation of the passivation layer. However, when it comes to reduced operating temperature SOFCs, such as a micro-SOFC (μSOFC), chemical or mechanical treatments can be expected to enhance cathode performance by kinetically freezing in the modified surface chemistry at reduced temperatures. Furthermore, as demonstrated in this work, Sr segregation can also be controlled by control of the Sr to B site ratio. Therefore, enhancements in k may be possible by carefully controlling etching conditions and/or electrode chemistry.

5. Conclusions

The surface chemical composition of dense thin film $SrTi_{1-x}Fe_xO_{3-\delta}$ electrodes, with considerably simplified electrode geometry, was investigated by means of XPS, focusing on surface cation segregation. An appreciable degree of Sr-excess was found at the surface of STF specimens over the wide composition range studied. Films with higher Fe fraction, x, were observed to exhibit considerably stronger Sr segregation. Depth and take-off angle dependent XPS spectra, in combination with chemical and thermal treatments, suggested that the Sr-excess is largely accommodated by the formation of RP phases or SrO island precipitates, possibly driven by mechanical strain gradients.

Furthermore, the degree of surface segregation was successfully controlled by etching the films, and/or preparing intentionally Sr deficient films. Studies of EIS measurements, under circumstances where surface chemistry was controlled, revealed the blocking effect of the segregation on the surface oxygen exchange rate. The insensitivity of the activation energy associated with the area specific resistance as measured by the electrode impedance R_{STF} points to one of two possible compatible models. Either the passivation layer exhibits some porosity or pin-holes enabling oxygen to reach the STF surface unhindered albeit at a considerably reduced active area or that the passivation layer is fully dense but electrons can tunnel from the STF electrode through the layer to the adsorbed oxygen. Further work, including scanning tunneling microscopy, is being initiated by the authors to address this interesting question.[51]

Acknowledgements

This work was initially supported by the Ceramics Program, Division of Materials Research Directorate for Mathematical & Physical Sciences, National Science Foundation under award DMR-0243993 and continued under the Materials Science and Engineering Division, Office of Basic Energy Sciences, Department of Energy under award DE SC0002633. W.J. Thanks the Samsung Foundation for fellowship support. The authors thank Dr R.A. De Souza and Dr J. Fleig for helpful discussions. The X-ray, XPS and AFM facilities of the Center for Materials Science and Engineering, an NSF MRSEC funded facility were used in this study.

Notes and references

1 N. Q. Minh, *J. Am. Ceram. Soc.*, 1993, **76**, 563–588.
2 S. M. Haile, *Acta Mater.*, 2003, **51**, 5981–6000.
3 R. M. Ormerod, *Chem. Soc. Rev.*, 2003, **32**, 17–28.
4 S. B. Adler, *Chem. Rev.*, 2004, **104**, 4791–4843.
5 D. J. L. Brett, A. Atkinson, N. P. Brandon and S. J. Skinner, *Chem. Soc. Rev.*, 2008, **37**, 1568–1578.
6 A. J. Jacobson, *Chem. Mater.*, 2010, **22**, 660–674.
7 J. Richter, P. Holtappels, T. Graule, T. Nakamura and L. J. Gauckler, *Monatsh. Chem.*, 2009, **140**, 985–999.
8 J. Fleig, F. S. Baumann, V. Brichzin, H. R. Kim, J. Jamnik, G. Cristiani, H. U. Habermeier and J. Maier, *Fuel Cells*, 2006, **6**, 284–292.
9 M. Mogensen, K. V. Jensen, M. J. Jørgensen and S. Primdahl, *Solid State Ionics*, 2002, **150**, 123–129.
10 N. Caillol, M. Pijolat and E. Siebert, *Appl. Surf. Sci.*, 2007, **253**, 4641–4648.
11 J. Jamnik and J. Maier, *Phys. Chem. Chem. Phys.*, 2001, **3**, 1668–1678.
12 W. Jung and H. L. Tuller, *J. Electrochem. Soc.*, 2008, **155**, B1194–B1201.
13 W. Jung and H. L. Tuller, *Solid State Ionics*, 2009, **180**, 843–847.
14 W. Jung and H. L. Tuller, *Adv. Energy Mater.*, 2011, DOI: 10.1002/aenm.201100164.
15 P. V. Nagarkar, P. C. Searson and F. D. Gealy Iii, *J. Appl. Phys.*, 1991, **69**, 459–462.
16 NIST. Data. Gateway, NIST.
17 W. D. Yang, *J. Mater. Sci.*, 1999, **34**, 3533–3544.
18 S. Azad, M. H. Engelhard and L.-Q. Wang, *J. Phys. Chem. B*, 2005, **109**, 10327–10331.
19 F. Voigts, C. Argirusis and W. Maus-Friedrichs, *Surf. Interface Anal.*, 2011, DOI: 10.1002/sia.3802.
20 F. Voigts, C. Argirusis and W. Maus-Friedrichs, *Surf. Interface Anal.*, 2011, **43**, 984–992.
21 E. Heifets, S. Piskunov, E. A. Kotomin, Y. F. Zhukovskii and D. E. Ellis, *Phys. Rev. B*, 2007, **75**, 13.
22 T. Kubo and H. Nozoye, *Surf. Sci.*, 2003, **542**, 177–191.
23 H. Wei, L. Beuermann, J. Helmbold, G. Borchardt, V. Kempter, G. Lilienkamp and W. Maus-Friedrichs, *J. Eur. Ceram. Soc.*, 2001, **21**, 1677–1680.
24 N. G. Eror and U. Balachandran, *J. Solid State Chem.*, 1982, **42**, 227–241.
25 S. N. Ruddlesden and P. Popper, *Acta Crystallogr.*, 1958, **11**, 54–55.
26 S. Sturm, M. Shiojiri and M. Ceh, *J. Mater. Res.*, 2011, **24**, 2596–2604.
27 K. R. Udayakumar and A. N. Cormack, *J. Phys. Chem. Solids*, 1989, **50**, 55–60.
28 K. Szot and W. Speier, *Phys. Rev. B: Condens. Matter*, 1999, **60**, 5909.
29 K. Szot, W. Speier, J. Herion and C. Freiburg, *Appl. Phys. A: Mater. Sci. Process.*, 1996, **64**, 55–59.
30 S. Witek, D. M. Smyth and H. Pickup, *J. Am. Ceram. Soc.*, 1984, **67**, 372–375.
31 H. Dulli, P. A. Dowben, S. H. Liou and E. W. Plummer, *Phys. Rev. B: Condens. Matter*, 2000, **62**, R14629.
32 Y. Liang and D. A. Bonnell, *Surf. Sci.*, 1994, **310**, 128–134.
33 K. Hawkins and T. J. White, *Philos. Trans. R. Soc. London, Ser. A*, 1991, **336**, 541–569.
34 R. Courths, J. Noffke, H. Wern and R. Heise, *Phys. Rev. B: Condens. Matter*, 1990, **42**, 9127.
35 G. Horvath, J. Gerblinger, H. Meixner and J. Giber, *Sens. Actuators, B*, 1996, **32**, 93–99.
36 R. Christian and C. J. William, *J. Am. Ceram. Soc.*, 1995, **78**, 2593–2602.
37 D. Monceau, C. Petot and G. Petot-Ervas, *Solid State Ionics*, 1991, **45**, 231–237.
38 R. Wang, Y. Zhu and S. M. Shapiro, *Phys. Rev. Lett.*, 1998, **80**, 2370.
39 C. Reinke and W. C. Johnson, *J. Am. Ceram. Soc.*, 1995, **78**, 2593–2602.
40 R. D. Shannon, *Acta Crystallogr., Sect. A: Cryst. Phys., Diffr., Theor. Gen. Crystallogr.*, 1976, **32**, 751.
41 H. Yokokawa, N. Sakai, T. Kawada and M. Dokiya, *Solid State Ionics*, 1992, **52**, 43–56.
42 D. P. Fagg, V. V. Kharton, A. V. Kovalevsky, A. P. Viskup, E. N. Naumovich and J. R. Frade, *J. Eur. Ceram. Soc.*, 2001, **21**, 1831–1835.
43 M. Vracar, A. Kuzmin, R. Merkle, J. Purans, E. A. Kotomin, J. Maier and O. Mathon, *Phys. Rev. B*, 2007, 76.

44 S. P. Jiang and J. G. Love, *Solid State Ionics*, 2001, **138**, 183–190.
45 G. J. la O', R. F. Savinell and Y. Shao-Horn, *J. Electrochem. Soc.*, 2009, **156**, B771–B781.
46 S. F. Wagner, C. Warnke, W. Menesklou, C. Argirusis, T. Damjanovic, G. Borchardt and E. Ivers-Tifee, *15th International Conference on Solid State Ionics*, Baden Baden, Germany, 2006.
47 E. Mutoro, E. J. Crumlin, M. D. Biegalski, H. M. Christen and Y. Shao-Horn, *Energy Environ. Sci.*, 2011, **4**, 3689–3696.
48 C. A. J. Fisher and M. S. Islam, *J. Mater. Chem.*, 2005, **15**, 3200–3207.
49 C. Navas, H. L. Tuller and H.-C. z. Loye, *J. Eur. Ceram. Soc.*, 1999, **19**, 737–740.
50 Y. A. Shilova, M. V. Patrakeev, E. B. Mitberg, I. A. Leonidov, V. L. Kozhevnikov and K. R. Poeppelmeier, *J. Solid State Chem.*, 2002, **168**, 275–283.
51 Y. Chan, W. Jung, Y. Kuru, H. L. Tuller and B. Yildiz, *ECS Trans.*, 2011, **35**, 2409–16.

